



Effect of Nb on Austenite Grain Growth in 10Cr-3Co-2W Martensitic Heat-Resistant Steel

Bong Cheon Park^{1,4} · Sung-Dae Kim² · Ihho Park¹ · Jong-Ho Shin³ · Jae Hoon Jang¹  · Namhyun Kang⁴

Received: 18 March 2024 / Accepted: 17 May 2024
© The Author(s) 2024

Abstract

The effect of Nb on austenite grain growth kinetics was investigated in 10Cr-3Co-2W martensitic heat-resistant steel under various tempering conditions (temperature and time). The results demonstrate that Nb effectively refines the austenite grain size; this result is attributed to the combined effect of Nb atom solute drag effect and pinning effect of NbC precipitates. Based on the measured values, an empirical model was developed to predict the grain growth behavior of this alloy system. In addition, the key conditions and parameters for application to the microstructure evolution model of MatCalc software were derived. Results will enable the prediction of grain size at different Nb contents and temperature parameters, and provide useful information for designing heat treatment processes and alloys.

Keywords Austenite · Grain growth · Heat resistant steel · Modeling

1 Introduction

Ferritic/martensitic 9–12 wt% Cr heat-resistant steels, due to their high creep resistance, low thermal expansion coefficient, high thermal conductivity, and high-temperature oxidation resistance [1–3], have been studied widely as materials for steam turbine components in ultra-supercritical (USC) power plants [4, 5]. The manufacturing process of steam turbine components typically involves multiple heat treatment steps, including preliminary heat treatment, quality heat treatment, and stress relieving heat treatment, along with forging and cutting to create the desired shape [6]. The heating parameters (temperature and time) of hot working and heat treatment processes significantly affect austenite

grain sizes. The prior austenite grain size (PAGS) during heating affects the substructure of the final tempered martensite microstructure, which in turn determines creep resistance [7]. Therefore, controlling PAGS during heat treatment is a key strategy for enhancing creep resistance. Investigating the effects of heating parameters on austenite grain refinement and analyzing the austenite grain growth mechanism are essential for developing alloys and processes for long-term operation at higher temperature [8].

Austenite grain growth behavior has been extensively studied for various materials [9–11]. Beck first reported an empirical model for grain growth in pure metals and alloys [12]. Subsequent studies on alloy systems revealed different behaviors compared to those of pure metals due to solute drag and Zener pinning effects [13–15]. Yue et al. investigated the austenite grain growth size and distribution evolution during long-term and high-temperature homogenization heat treatment of bearing steel [16]. Fernandez et al. calculated the solubility of carbides and nitrides in the austenite matrix and analyzed the effect of precipitates on austenite grain growth [17]. Azghandi and Flores et al. investigated the austenite grain growth of Ti-V and V-Nb added micro-alloyed steels under various isothermal conditions and proposed mathematical models dictating austenite grain growth [18, 19]. While many researchers have investigated the austenite grain growth behavior of various alloys in high-temperature environments, most studies focused on

✉ Jae Hoon Jang
jhjang@kims.re.kr

✉ Namhyun Kang
nhkang@pusan.ac.kr

¹ Department of Materials Analysis, Korea Institute of Materials Science, Changwon 51508, Republic of Korea

² Department of Materials Science and Engineering, Pukyong National University, Busan 48513, Republic of Korea

³ Corporate Research and Development Institute, Doosan Enerbility, Changwon 51711, Republic of Korea

⁴ Department of Materials Science and Engineering, Pusan National University, Busan 46241, Republic of Korea

specific alloys, limiting their applicability to other alloys. In particular, there are limited reports on the austenite grain growth behavior of ferritic/martensitic heat-resistant 9–12 wt% Cr steel [20].

This study investigates the austenite grain growth behavior of 10Cr-3Co-2W steel, developed for USC power plant rotors, through a series of isothermal heat-treatments. Based on the measured austenite grain size, the coefficients of the model, determined based on Sellars' empirical model for grain growth, were derived [21]. The effects of heat treatment parameters such as temperature and holding time on austenite grain growth were analyzed, and the effect of Nb was quantified by comparing alloys with different Nb contents. Finally, key parameters of the grain growth model implemented in MatCalc software were derived to predict the effect of Nb atom and NbC precipitate on austenite grain growth. This allows predicting of the grain size during not only isothermal heat-treatment but also heating and cooling treatment of the alloy.

2 Materials and Experimental Method

To investigate the influence of Nb contents, two kinds of ferritic/martensitic 10 wt% Cr-based heat-resistant steel were designed that have similar chemical compositions except for Nb contents. The composition ranges of the investigated heat-resistant steels are given in Table 1. The two alloys were labeled 0Nb and 5Nb according to their Nb content. The composition range of the 5Nb alloys fell within that of the MTR10A steel, which was designed for use as a rotor in USC power plants in environments above 600 °C [22, 23]. The 0Nb alloy without Nb and the 5Nb alloy with 0.05 wt% Nb were designed to investigate the effect of Nb content on austenite grain kinetics.

60 kg ingots were fabricated by vacuum induction melting (VIM); these were then remelted through an electroslag remelting (ESR) process, followed by hot-forging. The hot-forged samples were machined in cube form (10 mm × 10 mm × 5 mm thickness) for heat treatment. The heat treatments were carried out in a conventional box furnace; samples were protected by sealing them in quartz tubes filled with a partial pressure of argon. The heat treatment schedule is shown in Fig. 1; process was designed to investigate prior austenite grain growth kinetics. A homogenization heat

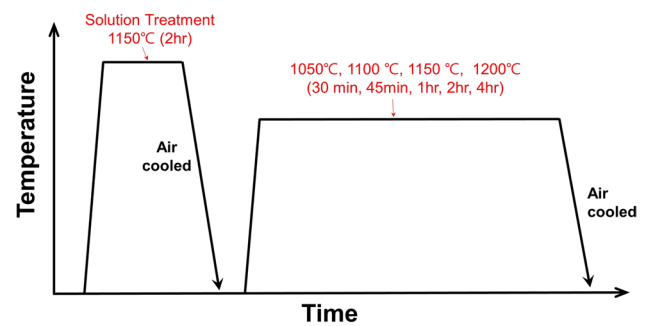


Fig. 1 Schematic diagram showing the two-step heat treatment. The first heating temperature, 1150 °C, was set to resolve NbC precipitation; the second heating temperature and holding time were determined to investigate austenite grain growth kinetics during isothermal holding

treatment was carried out at 1150 °C for 2 h in a box furnace. To investigate the austenite grain growth kinetics, isothermal holding was conducted at 1050, 1100, 1150, and 1200 °C for 30 min, 45 min, 1 h, 2 h, and 4 h, respectively. After each heat treatment, the specimens were air cooled.

During cooling, phase of specimens changed to martensite from austenite, and special care was required to measure the PAGS in the final martensitic microstructure [24]. To this end, this study used electron backscatter diffraction (EBSD) methods to reconstruct the prior austenite grain boundary, thermal etching (TE) method and chemical etching (CE) method.

(1) For the EBSD method, the specimens were polished with 1 μm diamond paste and finish-polished using a colloidal silica solution. They were then analyzed using the EBSD system attached to a scanning electron microscope (SEM, model JSM-7001F, JEOL). The EBSD patterns were acquired under the following conditions: acceleration voltage of 20 kV, specimen tilt of 70 degrees, and scan step size of 0.2 μm. Individual scan covers a surface of 240 μm × 180 μm. An approach based on the phase transformation orientation relationship was applied to reconstruct prior austenite orientation [25]. (2) By heat treating a finely polished specimen at a temperature in the austenite region to create grooves on the surface along the austenite grain boundaries, TE method is used to observe austenite grains [24]. Before heat treatment, the specimens were polished with 1 μm diamond paste and then sealed in a quartz tube under a vacuum of less than 10⁻³ torr. After TE method, the surface microstructure was observed using SEM. (3) CE method was performed after an additional tempering heat treatment at 650 °C for 2 h. The heat-treated specimens were fine-polished with 1 μm diamond paste and then etched using Vilella's reagent (100 ml of ethyl alcohol + 5 ml of HCL + 1 g of picric acid). The etched specimens were observed by SEM. The average austenite grain size was quantified using

Table 1 Chemical composition ranges of investigated heat-resistant steels (in wt%)

Label	C	Cr	W	Co	Nb
0Nb	0.08–0.14	9.70–10.70	1.55–1.85	3.0–4.0	< 0.001
5Nb	0.08–0.14	9.70–10.70	1.55–1.85	3.0–4.0	0.05

an Image analyzer (Image-Pro 7.0) for more than 5 images of the each heat-treated specimen.

The heat-treated specimens were observed using a transmission electron microscope (TEM; JEOL, JEM2100F) to observe the prior austenite grain boundary and precipitates. The TEM specimens were prepared by jet-polishing using a solution of methanol and perchloric acid mixed at a ratio of 9:1 after mechanical polishing.

3 Results

Figure 2 shows microstructures after the reheating steps at 1050 °C for 30 min for the 0Nb alloys. As expected, the microstructures were fully martensitic. The results measured using EBSD, CE, and TE methods showed similar sizes within the error range. This confirmed the reliability of each method for quantifying the PAGS. For measurements of PAGS at other temperatures and holding times, the CE method was used because it is relatively easy to prepare the specimens.

To analyze the austenite grain growth behavior, PAGS was measured over time at different temperatures. Figure 3 shows the microstructures of the 0Nb and 5Nb alloys after heat treatment at 1100 °C for 30 min and 4 h. Figure 4 summarizes the changes in PAGS for the 0Nb and 5Nb alloys at different temperatures and times. In the 0Nb alloy, the average grain sizes were 98.5, 107.7, 176.8, and 203.3 μm after heat treatment at 1050, 1100, 1150, and 1200 °C for 30 min,

respectively. The average grain sizes in the 5Nb alloys after heat treatment at 1050, 1100, 1150, and 1200 °C for 30 min were 40.3, 46.5, 105.0, and 171.8 μm , respectively. The initial state ($t = 0$) of grain growth was assumed to be at 30 min of heat treatment. The austenite grain size measured after 30 min of heat treatment for each alloy and temperature was assumed to be the initial austenite grain size, D_0 . The time applied for grain growth was set at the relative heat treatment time from the initial state.

Both alloys showed increases in austenite grain size with increasing time and temperature. In the time scale of heat treatment of interest in this study, the difference in grain size due to heat treatment temperature was more significant than that due to time, which is consistent with previous studies [16, 20, 26]. The 5Nb alloys showed a smaller grain size than that of the 0Nb alloy under the same conditions. This is attributed to the significant solute drag effect exhibited by solute Nb and the Zener pinning effect caused by the formation on NbC [27, 28]. In the case of holding at 1200 °C for 4 h, the grain sizes were $307.2 \pm 44.3 \mu\text{m}$ and $298.4 \pm 30.3 \mu\text{m}$ for 0Nb and 5Nb alloys, respectively, showing similar sizes between the two alloys. In contrast, at 1100 °C, the grain sizes after 4 h of isothermal holding were $165.8 \pm 31.7 \mu\text{m}$ and $81.9 \pm 15.6 \mu\text{m}$ for 0Nb and 5Nb alloys, respectively, showing a difference of about 2 times. This is because NbC mainly formed and pinned the grain growth at this temperature.

Figure 5 shows the calculated equilibrium phase fractions as a function of temperature for the 5Nb alloy using

Fig. 2 Microstructure of 0Nb alloys holding at 1050 °C for 30 min. **a** Electron back scatter diffraction image **b** Scanning electron microscopy results using thermal etching method **c** Scanning electron microscopy results using chemical etching method without tempering **d** Scanning electron microscopy results using chemical etching method after tempering at 650 °C for 2 h

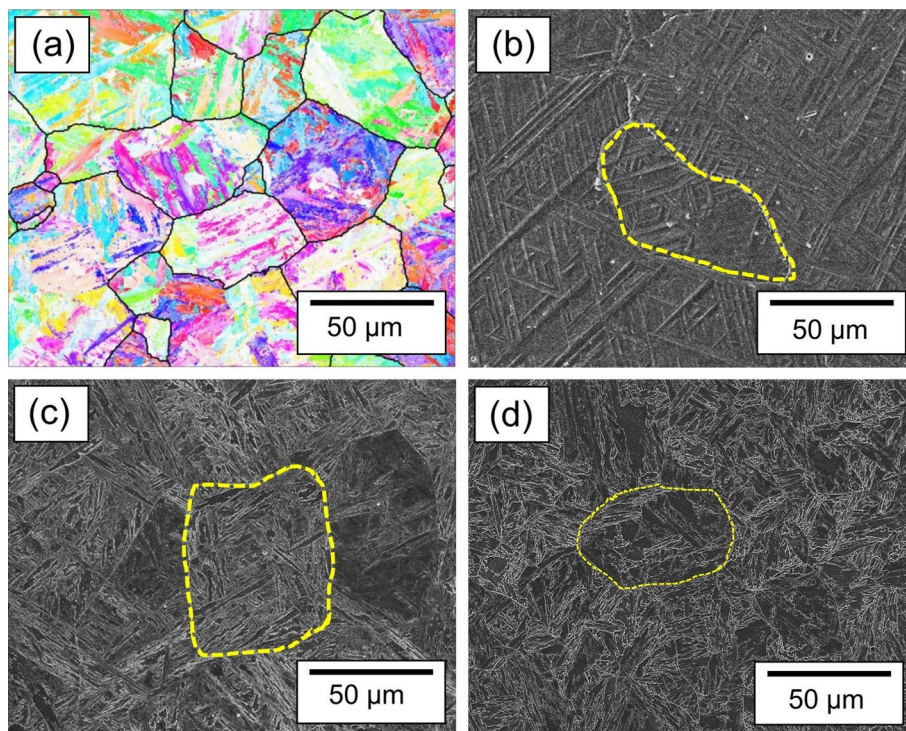


Fig. 3 SEM images of 0Nb and 5Nb alloys after heat treatment at 1100 °C: **a** 0Nb for 30 min **b** 0Nb for 4 h **c** 5Nb for 30 min **d** 5Nb for 4 h

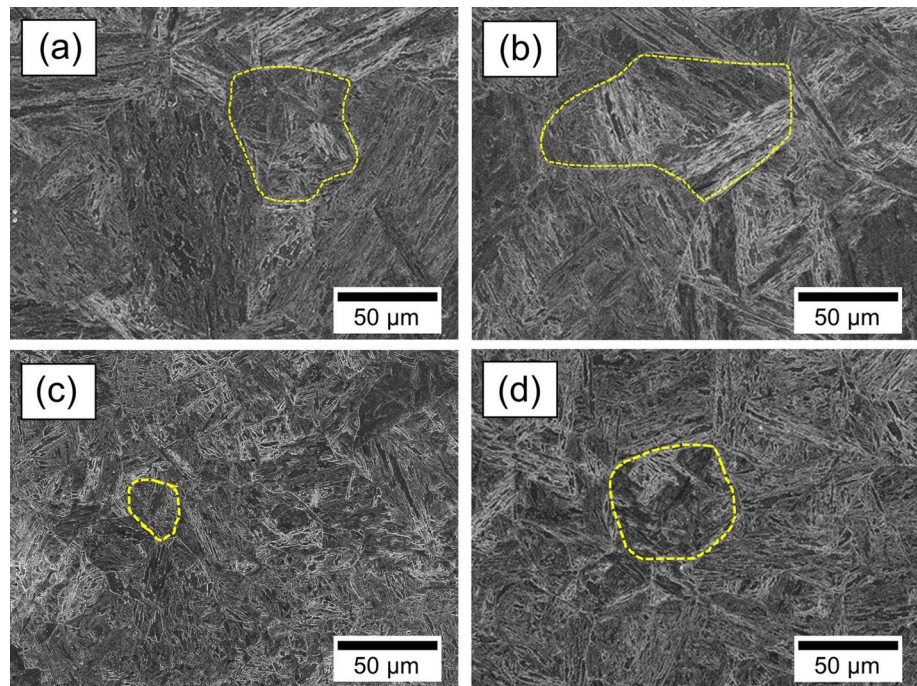


Fig. 4 Experimentally measured austenite grain sizes of **a** 0Nb and **b** 5Nb alloys during isothermal holding at different temperatures. The black squares, red diamonds, blue circles, and green triangles represent the measured austenite grain sizes after heat treatment at 1050, 1100, 1150, and 1200 °C, respectively

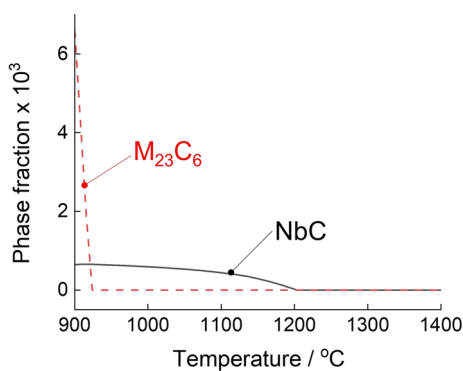
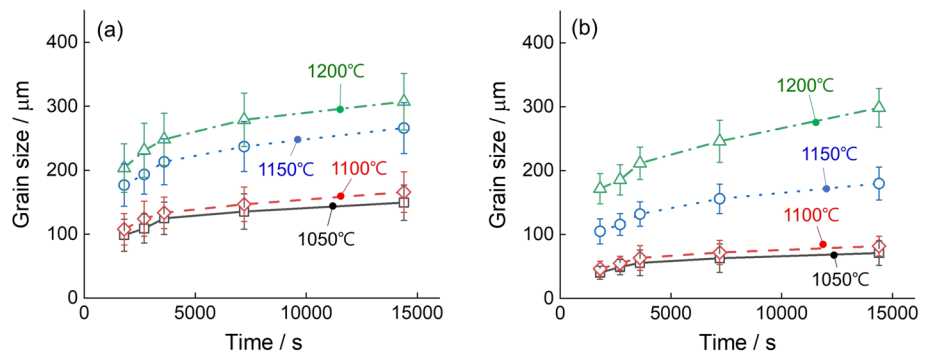


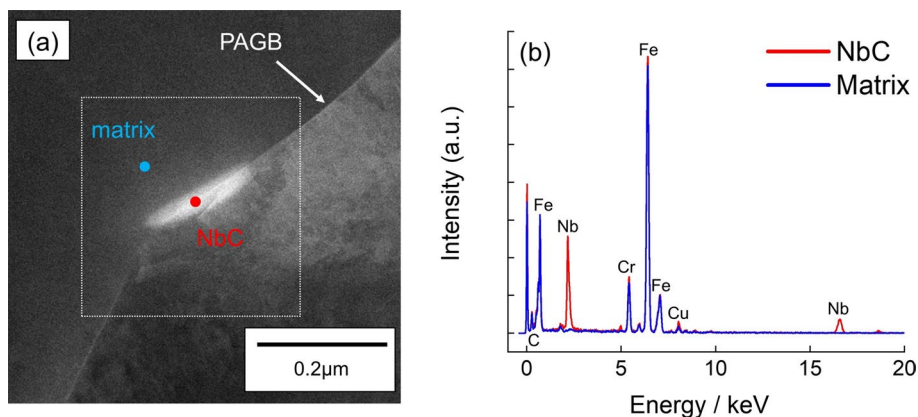
Fig. 5 Phase fractions of $M_{23}C_6$ and NbC precipitate of 5Nb alloys as a function of temperature, calculated using MatCalc software

the Gibbs energy database for steels (mc_steel, version 2.06), employing MatCalc software [29]. FCC and $M_{23}C_6$, NbC phases were allowed in the calculation. $M_{23}C_6$ is

a Cr-rich carbide with a complete dissolution temperature of approximately 930 °C. NbC starts to dissolve at 900 °C and is completely dissolved at 1200 °C. It is expected that a sufficient amount of NbC precipitates will survive in the region below 1100 °C, resulting in a sufficient pinning effect.

Figure 6a shows the microstructure of the 5Nb alloys after holding at 1100 °C for 1 h, observed by high-angle annular dark field scanning transmission electron microscopy (HAADF-STEM). Rod-shaped precipitate are located at the prior austenite grain boundary, and EDS analysis in Fig. 6b confirmed that these are NbC. The presence of a large number of NbC precipitates in the 5Nb alloy is thought to be responsible for the small grain size compared to that of the 0Nb alloy. These precipitates pin the austenite grain boundary, preventing it from moving and growing. This is consistent with previous research on micro-alloyed steels [28].

Fig. 6 **a** HAADF-STEM images of prior austenite grain boundary of 5Nb alloys after holding at 1100 °C for 1 h and **b** EDS spectrum analysis of matrix and NbC precipitate



4 Discussion

In this section, the austenite grain growth behavior of the 0Nb and 5Nb alloys is modeled using two different approaches. (1) An empirical model based on the time exponent and activation energy is used to predict the grain size evolution as a function of time and temperature. (2) MatCalc microstructure evolution model is used to take into account the solute drag effect of Nb and the pinning effect of NbC precipitates.

4.1 Empirical Model

The mathematical model for austenite grain growth kinetics in alloys was derived first by Beck and has been used in various studies with the empirical equation for the alloy [21], as shown in following form.

$$D^n - D_0^n = K \cdot t = k_0 \exp\left(-\frac{Q}{kT}\right) \cdot t \quad (1)$$

where D is the average grain size (μm), D_0 is the initial grain size, t is the time, n is the time exponent, Q is the

activation energy, and T is the isothermal heat treatment temperature. Different n , k_0 , and Q values have been reported for various alloys, reflecting the underlying physical metallurgy [30–35].

Assuming $D \gg D_0$,

$$D^n \approx K \cdot t \quad (2)$$

$$n \ln D \approx \ln t + \ln K. \quad (3)$$

The time exponent n can be derived from the relationship between $\ln D$ and $\ln t$. The average $n = 4.38$ was derived based on the grain size data of 0Nb and 5Nb alloys at each temperature. Typically, n is higher than 2 for alloys [33, 36] and, in this study, the value was higher than 2 due to the presence of multiple alloying elements.

Figure 7a and b show the plots of $D^n - D_0^n$ versus time for 0Nb and 5Nb alloys, respectively, using the previously obtained n values and the measured D_0 . A linear relationship is observed for each alloy and temperature, and the constant K is determined from the slope of the lines. Figure 7c shows $\ln K$ as a function of the reciprocal of temperature, $1/T$, for 0Nb and 5Nb alloys. From the linear relationship between

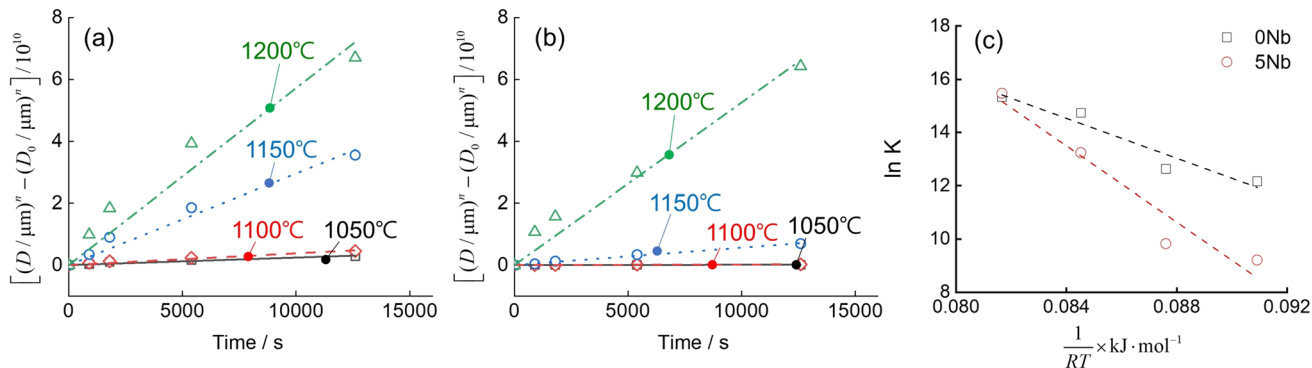


Fig. 7 Definition of fitting curve of grain size versus time at different temperatures for **a** 0Nb and **b** 5Nb alloys. **c** Fitting curves for $\ln K$ and $1/T$ to determine constant k_0 and activation energy Q

In K and $1/T$, the k_0 and Q values for each alloy were derived and are summarized in Table 2. The activation energy values for the 0Nb and 5Nb alloys are $375.4 \text{ kJ mol}^{-1}$ and $714.2 \text{ kJ mol}^{-1}$, respectively, which are within the range of $250\text{--}914 \text{ kJ mol}^{-1}$ for conventional alloy steels [21, 32]. The activation energy of the 0Nb alloy shows a value similar to the activation energy value of the HSLA steel grade reported in previous studies, considering the error range [37]. Although the 0Nb alloy contains a large quantity of alloying elements such as Cr and Co compared to HSLA steel, it is understood that these elements do not significantly affect activation energy in the temperature range of $1000\text{--}1200 \text{ }^\circ\text{C}$. The higher activation energy in 5Nb alloys indicates that the grain growth in 5Nb alloys is more sensitive to temperature changes than that in 0Nb alloy. This is because the amount of NbC precipitates increases as temperature decreases in 5Nb alloy, and this reflects addition effect of suppressing grain growth at lower temperature. Figure 8 shows the grain size predicted using the values of k_0 and Q given in Table 2 with the measured data for 0Nb and 5Nb alloys. The predicted grain size evolution agrees well with the measured data for both alloys within the error range.

4.2 MatCalc Microstructure Evolution Model

Empirical models similar to Beck's model can predict the grain growth behavior of a given alloy under heat treatment conditions. However, it has limitations in quantifying the effect of Nb on physical metallurgy. Therefore, a method of grain growth modeling that incorporates solute drag and Zener pinning effects is needed. Numerous studies have investigated grain growth models that consider physical metallurgy principles [20, 37, 38]. This study utilizes the microstructure evolution model in MatCalc software to incorporate the solute drag effect of Nb atoms and the

pinning effect of NbC precipitates. The model is based on the following equation, which considers the driving force (P_d) for grain growth, and the retardation force (P_r) due to solute drag, and the precipitate pinning.

$$\frac{dD}{dt} = M \cdot (P_d - P_r) \quad (4)$$

The derivation of the model and the meaning of each parameter are described in the previous paper [39]. The evolution of grain size was simulated using the microstructure evolution model of MatCalc software. The Gibbs energy database (mc_steel, version 2.06) and mobility database (mc_steel, version 2.012) for steels were used to simulate the precipitation and grain size evolution. The solute drag effect of alloying elements other than Nb atoms was applied as the value that well predicts the grain growth behavior of 0Nb alloy considering the segregation energy of the Cr atom, which has the highest alloy content. Referring to the existing literature, the values of the parameters were applied as shown in Table 3.

Figure 9 compares the simulated and measured grain size evolution for 0Nb and 5Nb alloys. The initial grain size at each temperature was assumed to be the grain size after 30 min of heat treatment. Figure 9a shows the simulated

Table 2 Empirical model parameters

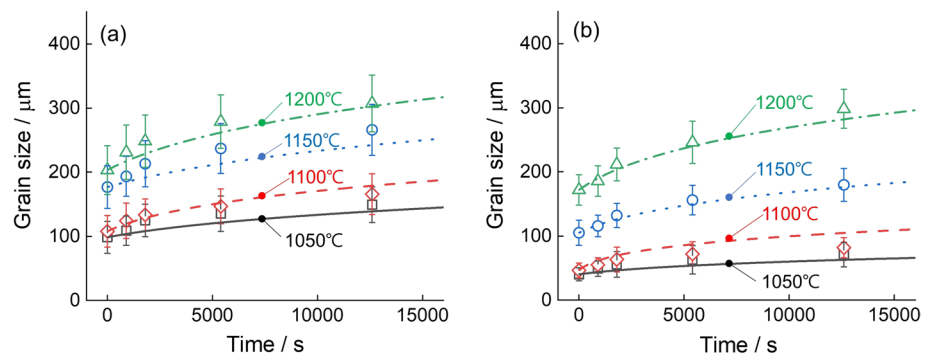
label	$\ln k_0$	$Q / \text{kJ mol}^{-1}$
0Nb	46.07	375.4
5Nb	73.49	714.2

Table 3 Parameters of microstructure evolution model implemented in MatCalc software

Parameter	Value	References
M_0	$120 \text{ m}^4 / \text{J s}$	[40]
Q	386 kJ mol^{-1}	[37]
γ_g	0.5 J m^{-2}	[40]
k_d	4	[41]
k_r	4	[41]
E_{Nb}	38 kJ mol^{-1}	[42]
E_{Cr}	7.9 kJ mol^{-1}	This work

M_0 is the pre-exponential mobility factor, Q is the activation energy of the mobility, γ_g is the grain boundary energy, k_d and k_r are the driving and retarding force parameter determined according to Zener theory. E_{Nb} and E_{Cr} are the solute drag interaction energy of Nb and Cr

Fig. 8 Comparison of empirical model predicted and experimentally obtained grain growth kinetics in **a** 0Nb and **b** 5Nb alloys



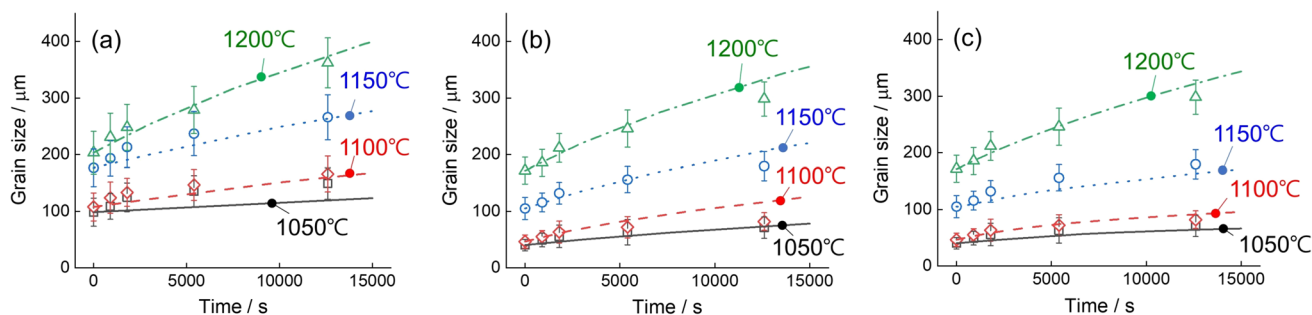


Fig. 9 Comparison of physical model calculated using MatCalc software and experimentally obtained grain growth kinetics in **a** 0Nb alloy and 5Nb alloy **b** without and **c** with Zener pinning effect

grain size evolution for the 0Nb alloy. The results are in good agreement with the measured data, within an error range. Figure 9b compares the simulated grain size evolution for the 5Nb alloy. Due to the solute drag effect of Nb atoms, the 5Nb alloy shows a smaller grain size than that of the 0Nb alloy at the same temperature and heat treatment time. The simulated results match well with the results measured above 1150 °C, but overestimate the grain size at 1100 °C.

This overestimation can be explained by the presence of a certain amount of NbC precipitates below this temperature, as can be inferred by thermodynamic calculations and microstructure observations. These precipitates pin the austenite grain growth, resulting in a smaller grain size. To simulate this effect, the grain growth behavior was simulated assuming an initial distribution of NbC precipitates with equilibrium volume fraction of 6.5×10^{-4} at 900 °C and average size 20 nm. This precipitate distribution was obtained by simulating precipitation kinetics for 3×10^7 seconds at an isothermal heat treatment condition of 900 °C. The simulated grain size results show a similar grain size to that without considering the pinning effect at 1200 °C. However, below 1150 °C, the grain size is simulated and found to be smaller than that without considering the pinning effect,

which leads to a better match with the measured results at 1100 °C.

Figure 10 summarizes the evolution of precipitate fraction and size during isothermal heat treatment. At 1200 °C, the equilibrium volume fraction of NbC precipitates is close to zero. The precipitates dissolve at the beginning of the heat treatment, and there is little pinning effect on grain growth. However, below 1150 °C, a certain amount of NbC precipitates remains, and their size does not grow significantly. Therefore, the precipitates can pin the grain growth. This effect is more pronounced at lower temperatures because the equilibrium volume fraction of precipitates is higher. In the alloys studied in this work, the effect of Nb is a combination of solute drag effect of Nb atoms and pinning effect of NbC precipitates.

5 Conclusion

In this study, the effect of Nb on the austenite grain growth behavior of 10Cr-3Co-2W martensitic heat-resistant steel was investigated. The main results are as follows. Nb addition refines the austenite grain size during

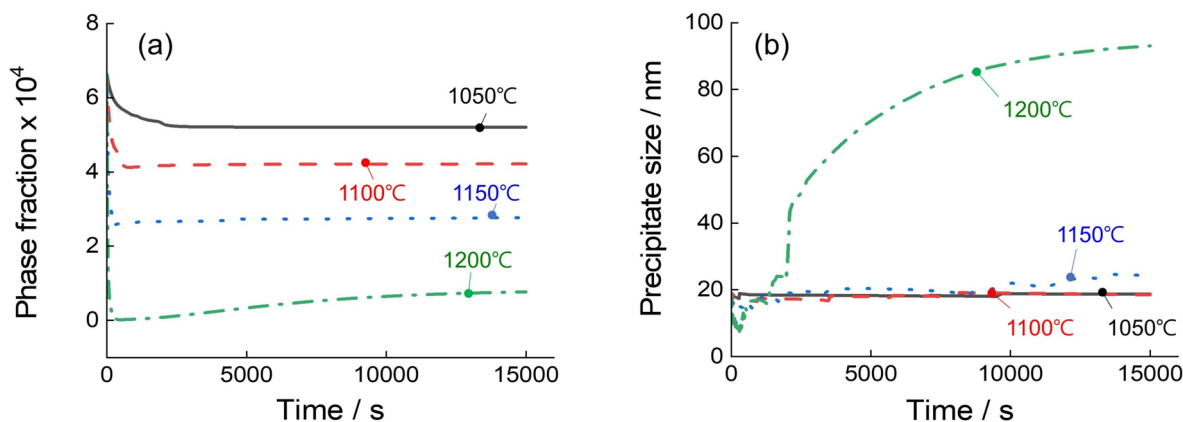


Fig. 10 **a** Phase fraction and **b** precipitate size of NbC in 5Nb alloy, calculated as a function of time using MatCalc software

isothermal heat treatment in the temperature range of 1050–1200 °C. A Beck's type equation yielded values of $k_0 = \exp(46.07)$ and $Q = 375.4 \text{ kJ mol}^{-1}$ for the Nb-free steel and $k_0 = \exp(73.49)$ and $Q = 714.2 \text{ kJ mol}^{-1}$ for the Nb-added steel. The MatCalc microstructure evolution model successfully simulated the grain growth behavior, considering both the solute drag effect of Nb atoms and the pinning effect of NbC precipitates. The pinning effect of NbC precipitates was identified as the major factor retarding the austenite grain growth below 1100 °C.

Acknowledgements This work was funded by the Fundamental R & D Program of the Korea Institute of Materials Science (KIMS), Grant No. PNK9630. This work was also supported by the Industrial Strategic Technology Development Program (No. 20010778 & 20010942) funded by the Ministry of Trade, Industry & Energy (MOTIE, Korea).

Declarations

Conflict of interest The author declare that they have no known competing financial interests or personal relationship that could have appeared influence the work reported in this paper.

Open Access This article is licensed under a Creative Commons Attribution 4.0 International License, which permits use, sharing, adaptation, distribution and reproduction in any medium or format, as long as you give appropriate credit to the original author(s) and the source, provide a link to the Creative Commons licence, and indicate if changes were made. The images or other third party material in this article are included in the article's Creative Commons licence, unless indicated otherwise in a credit line to the material. If material is not included in the article's Creative Commons licence and your intended use is not permitted by statutory regulation or exceeds the permitted use, you will need to obtain permission directly from the copyright holder. To view a copy of this licence, visit <http://creativecommons.org/licenses/by/4.0/>.

References

1. F. Abe, Precipitate design for creep strengthening of 9% Cr tempered martensitic steel for ultra-supercritical power plants. *Sci. Technol. Adv. Mater.* **9**(1), 013002 (2008)
2. P. Ennis, A. Czyrska-Filemonowicz, Recent advances in creep-resistant steels for power plant applications. *Sadhana* **28**, 709–730 (2003)
3. F. Abe, M. Taneike, K. Sawada, Alloy design of creep resistant 9Cr steel using a dispersion of nano-sized carbonitrides. *Int. J. Press. Vessels Pip.* **84**(1–2), 3–12 (2007)
4. B.O. Kong, M.S. Kim, B.H. Kim, J.H. Lee, Prediction of creep life using an explainable artificial intelligence technique and alloy design based on the genetic algorithm in creep-strength-enhanced ferritic 9% Cr steel. *Met. Mater. Int.* **29**(5), 1334–1345 (2023)
5. H. Yin, J. Zhao, H. Bao, W. Ge, F. Yin, R. Hu, H. Jia, Distribution of boron in 9.5 Cr-1.5 MoCoVNbNB martensitic heat-resistant steel studied by secondary ion mass spectroscopy and atom probe tomography. *Met. Mater. Int.* **30**(4), 990–1001 (2024)
6. F. Abe, T.-U. Kern, R. Viswanathan, *Creep-Resistant Steels* (Elsevier, Amsterdam, 2008)
7. X. Zhou, C. Liu, L. Yu, Y. Liu, H. Li, Phase transformation behavior and microstructural control of high-Cr martensitic/ferritic heat-resistant steels for power and nuclear plants: A review. *J. Mater. Sci. Technol.* **31**(3), 235–242 (2015)
8. S. Ju, H.H. Lee, J.-H. Shin, D.-W. Suh, Influence of partial replacement of Co with Cu on isothermal transformation kinetics in ferritic/martensitic heat-resistant steel. *Steel Res. Int.* **94**(2), 2200228 (2023)
9. H. Wang, W. Wang, Simple model for austenite grain growth in microalloyed steels. *Mater. Sci. Technol.* **24**(2), 228–232 (2008)
10. M. Pa, D. Dp, T. Chandra, K. Cr, Grain growth predictions in microalloyed steels. *ISIJ Int.* **36**(2), 194–200 (1996)
11. F. Najafkhani, S. Kheiri, B. Pourbahari, H. Mirzadeh, Recent advances in the kinetics of normal/abnormal grain growth: a review. *Arch. Civ. Mech. Eng.* **21**, 29 (2021)
12. P.A. Beck, J.C. Kremer, L. Demer, M. Holzworth, Grain growth in high-purity aluminum and in an aluminum-magnesium alloy. *Trans. Am. Inst. Min. Metall. Eng.* **175**, 372–400 (1948)
13. J.W. Cahn, The impurity-drag effect in grain boundary motion. *Acta Metall.* **10**(9), 789–798 (1962)
14. M. Hillert, On the theory of normal and abnormal grain growth. *Acta Metall.* **13**(3), 227–238 (1965)
15. C. Celada-Casero, J. Sietsma, M.J. Santofimia, The role of the austenite grain size in the martensitic transformation in low carbon steels. *Mater. Des.* **167**, 107625 (2019)
16. C. Yue, L. Zhang, S. Liao, H. Gao, Kinetic analysis of the austenite grain growth in GCr15 steel. *J. Mater. Eng. Perform.* **19**, 112–115 (2010)
17. A. Fernández, P. Uranga, B. Lopez, J. Rodriguez-Ibabe, Dynamic recrystallization behavior covering a wide austenite grain size range in Nb and Nb-Ti microalloyed steels. *Mater. Sci. Eng. A* **361**(1–2), 367–376 (2003)
18. S.H. Mohamadi Azghandi, V. Ghanooni Ahmadabadi, A. Zabet, F. Fazeli, Modelling of austenite grain growth kinetics in a microalloyed steel (30MSV6) in the presence of carbonitride precipitates. *Philos. Mag.* **94**(24), 2758–2775 (2014)
19. O. Flores, L. Martinez, Abnormal grain growth of austenite in a V-Nb microalloyed steel. *J. Mater. Sci.* **32**, 5985–5991 (1997)
20. Y. Xu, J. Liu, Y. Zhao, Y. Jiao, Austenite grain growth kinetics and mechanism of grain growth in 12Cr ultra-super-critical rotor steel. *Phil. Mag.* **101**(1), 77–95 (2021)
21. C.M. Sellars, J.A. Whiteman, Recrystallization and grain growth in hot rolling. *Metal Sci.* **13**(3–4), 187–194 (1979)
22. F. Abe, Development of creep-resistant steels and alloys for use in power plants, in *Structural alloys for power plants*. (Elsevier, Amsterdam, 2014), pp.250–293
23. F. Abe, M. Tabuchi, S. Tsukamoto, Alloy design of MARBN for boiler and turbine applications at 650 oC. *Mater. High Temp.* **38**(5), 306–321 (2021)
24. C.G. De Andres, M. Bartolomé, C. Capdevila, D. San Martin, F. Caballero, V. López, Metallographic techniques for the determination of the austenite grain size in medium-carbon microalloyed steels. *Mater. Charact.* **46**(5), 389–398 (2001)
25. M. Abbasi, T.W. Nelson, C.D. Sorensen, L. Wei, An approach to prior austenite reconstruction. *Mater. Charact.* **66**, 1–8 (2012)
26. G. Ji, X.-H. Gao, Z.-G. Liu, K. Zhang, In situ observation and modeling of austenite grain growth in a Nb-Ti-bearing high carbon steel. *J. Iron. Steel Res. Int.* **26**, 292–300 (2019)
27. A. Karmakar, S. Kundu, S. Roy, S. Neogy, D. Srivastava, D. Chakrabarti, Effect of microalloying elements on austenite grain growth in Nb-Ti and Nb-V steels. *Mater. Sci. Technol.* **30**(6), 653–664 (2014)
28. L. Fu, H. Wang, W. Wang, A. Shan, Austenite grain growth prediction coupling with drag and pinning effects in low carbon Nb microalloyed steels. *Mater. Sci. Technol.* **27**(6), 996–1001 (2011)
29. E. Kozeschnik, J. Svoboda, P. Fratzl, F. Fischer, Modelling of kinetics in multi-component multi-phase systems with spherical

- precipitates: II: numerical solution and application. *Mater. Sci. Eng. A* **385**(1–2), 157–165 (2004)
30. K. Matsuura, Y. Itoh, Analysis of the effect of grain size distribution on grain growth by computer simulation. *ISIJ Int.* **31**(4), 366–371 (1991)
 31. J.H. Beynon, C.M. Sellars, Modelling microstructure and its effects during multipass hot rolling. *ISIJ Int.* **32**(3), 359–367 (1992)
 32. S. Nanba, M. Kitamura, M. Shimada, M. Katsumata, T. Inoue, H. Imamura, Y. Maeda, S. Hattori, Prediction of microstructure distribution in the through-thickness direction during and after hot rolling in carbon steels. *ISIJ Int.* **32**(3), 377–386 (1992)
 33. H. Pd, A mathematical model to predict the mechanical properties of hot rolled C-Mn and microalloyed steels. *ISIJ Int.* **32**(12), 1329–1338 (1992)
 34. T. Senuma, Physical metallurgy of modern high strength steel sheets. *ISIJ Int.* **41**(6), 520–532 (2001)
 35. S.-J. Lee, Y.-K. Lee, Prediction of austenite grain growth during austenitization of low alloy steels. *Mater. Des.* **29**(9), 1840–1844 (2008)
 36. E. Anelli, Application of mathematical modelling to hot rolling and controlled cooling of wire rods and bars. *ISIJ Int.* **32**(3), 440–449 (1992)
 37. J. Moon, J. Lee, C. Lee, Prediction for the austenite grain size in the presence of growing particles in the weld HAZ of Ti-microalloyed steel. *Mater. Sci. Eng. A* **459**(1–2), 40–46 (2007)
 38. S. Depinoy, B. Marini, C. Toffolon-Masclat, F. Roch, A.-F. Gourgues-Lorenzon, Austenite grain growth in a 2.25 Cr-1Mo vanadium-free steel accounting for zener pinning and solute drag: experimental study and modeling. *Metall. Mater. Trans. A* **48**, 2289–2300 (2017)
 39. M. Rath, E. Kozeschnik, Coupled grain growth and precipitation modeling in multi-phase systems. *Mater. Sci. Forum* **753**, 357–360 (2013)
 40. K. Banerjee, M. Militzer, M. Perez, X. Wang, Nonisothermal austenite grain growth kinetics in a microalloyed X80 linepipe steel. *Metall. Mater. Trans. A* **41**, 3161–3172 (2010)
 41. P.R. Rios, Overview no. 62: A theory for grain boundary pinning by particles. *Acta Metall.* **35**(12), 2805–2814 (1987)
 42. P.J. Felfel, C.R. Killmore, J.G. Williams, K.R. Carpenter, S.P. Ringer, J.M. Cairney, A quantitative atom probe study of the Nb excess at prior austenite grain boundaries in a Nb microalloyed strip-cast steel. *Acta Mater.* **60**(13–14), 5049–5055 (2012)

Publisher's Note Springer Nature remains neutral with regard to jurisdictional claims in published maps and institutional affiliations.